



Numerical simulation of unsteady mixed convection of nanofluid in a lid-driven square cavity

Nagehan Alsoy-Akgün 

Department of Mathematics, Yüzüncü Yıl University, Van, Turkey

Abstract

The behavior of unsteady mixed convection flow of Cu -water based nanofluids is investigated numerically inside a square lid-driven partially heated flow below. Dual Reciprocity Boundary Element Method is used to solve stream function-vorticity form of the governing equations of the problem. The need of time integration scheme is eliminated by transforming the vorticity transport and energy equations to modified Helmholtz equations. This procedure also diminishes the stability problems. The numerical results are given for several values of Reynolds number (Re), Rayleigh number (Ra), heat source location (D), heat source length (B) and solid volume fraction (ϕ). The steady-state results are in good agreement with the results available in the literature.

Mathematics Subject Classification (2010). 35Q35, 35Q79

Keywords. DRBEM, nanofluid, lid-driven cavity

1. Introduction

Nanofluids are suspension of a base fluid (e.g. water, ethylene glycol and mineral oil etc.) with nano-sized particles ($\text{dia} < 100\text{nm}$) (e.g. copper (Cu), aluminium oxide (Al_2O_3), silver (Ag), titanium dioxide (TiO_2)). Adding nanoparticles into conventional heat transfer fluids with low thermal conductivity, their heat transfer performance and thermophysical properties can be enhanced. Due to the ability of high thermal conductivity, they are preferred in many engineering area such as cooling of electronics, cooling of diesel electric generators, cooling and heating in buildings etc. to increase the performance of the devices. A comprehensive literature review about nanofluid has been done in [12], [22], [27]-[30]. The important published articles on the enhancement of the forced convection heat transfer with nanofluids have been summarized in [12], applications and challenges of nanofluids have been compiled and reviewed in [22], recent research on theoretical and numerical investigations of various thermal properties and applications of nanofluids have been summarized in [27], fluid flow and heat transfer characteristics of nanofluids in forced and free convection flows and potential applications of nanofluids have been covered in [28], a critical review of research on heat transfer applications of nanofluids with the aim of identifying the limiting factors has been presented in [29] and a detailed literature review and an assessment of results of the research and development work forming the

current status of nanofluid technology for heat transfer applications have been presented and discussed in [30].

There are many studies about the mixed convection problem in a lid-driven cavity in the literature. In these studies, the effect of the parameters such as Reynolds number, Rayleigh number, and nanoparticle volume fraction on the flow are investigated using different geometry and changing the shape, length and location of the heater. Chamkha and Abu-Nada [7] numerically studied steady mixed convection flow in single and double-lid square cavities filled with a water- Al_2O_3 nanofluid using a second-order accurate finite-volume method. Another two numerical studies for steady mixed convection flow is investigated in lid-driven triangular enclosure filled with a water- Al_2O_3 by Ghasemi and Aminossadati in [9] using the power law profile approximation and SIMPLE algorithm and in lid-driven rectangular enclosure filled with a water- Al_2O_3 by Mahmoodi in [14] using the finite volume approach and SIMPLER algorithm. On the other hand, steady mixed convection flow in lid-driven rectangular and square cavities filled with a Cu -water nanofluid are studied by Muthitamilselvan et al. [16], Rahman et al. [20] and Talebi et al. [25] using the finite volume technique with SIMPLE algorithm, finite element method based on Galerkin-weighted residuals and finite volume method, respectively. A finite difference method are used in the work of Sheremet and Pop [24] for the solution of steady mixed convection in side a two sided lid-driven cavity filled with water based nanofluid. A numerical study is given for nanofluid with several nanoparticles such as Cu , CuO , Al_2O_3 in a lid-driven square cavity by Nemati et al. in [18] using the Lattice Boltzmann method.

The mixed convection in a partially heated square cavity filled with nanofluid is numerically analyzed in many works. Mansour et al. [15] and Salari et al. [23] are used finite difference method and finite volume computational procedure with SIMPLE algorithm, respectively, to investigate the effect of heat source by changing its location, size and shape using various nanoparticles such as Cu , Ag , Al_2O_3 and TiO_2 . Also, Tivari and Das [26] presented an unsteady problem in two sided lid driven square cavity using finite volume approach with SIMPLE algorithm. Lid-driven mixed convection with water- Al_2O_3 nanofluid inside a square enclosure with a hot rectangular obstacle at bottom is numerically studied by Esfe et al. in [8] using finite volume method. Another computational study for heat source with different geometry is done by Kalteh et al. in [13] using finite difference method. In this study, a triangular heat source is placed in the middle of the square cavity and Al_2O_3 , TiO_3 , Ag and CuO are used as nanoparticles.

Many studies about the effects of enclosure inclination angle on the heat transfer characteristics for mixed convection in a lid-driven inclined square enclosure filled with a nanofluid is presented in the literature. A numerical study about steady mixed convection flow of Al_2O_3 -water in a lid-driven inclined square enclosure using a second-order accurate finite-volume method is given by Abu-Nada and Chamkha in [1]. Rahman et al. [21] studied the behavior of Cu -water nanofluids in an inclined lid-driven triangular enclosure and Galerkin finite element method is used for numerical computations. Also, the behavior of water- Al_2O_3 in a double lid-driven square cavity with various inclination angles and discrete heat sources is investigated by Arani et al. in [4] and by Hussain et al. in [11]. In the discretization of unsteady governing equations finite element method in space and the Crank-Nicolson in time are used while in the discretization of steady governing equations finite volume computational procedure and the SIMPLE algorithm are used.

The effect of entropy generation due to heat transfer and to viscous effects investigated numerically for mixed convection flow in a square cavity with a moving lid filled with Cu -water nanofluid using the Lattice Boltzmann method by Bouchmel et al. in [5]. Another numerical study of entropy generation is done for mixed convection and heat transfer of a nanofluid inside a skew enclosure filled with Cu -water nanofluid using the finite volume based SIMPLER algorithm by Nayak et al. in [17].

As in mentioned above studies, mixed convection flow of nanofluids has been studied in different geometries and using several numerical methods which are the domain discretization methods. Discretization of the whole domain of the problem causes very large system of algebraic equations and needs extra computational effort. Differently, dual reciprocity boundary element method (DRBEM) needs only the discretization of the boundary of the domain which is the main advantages of the method. DRBEM is a very suitable method for the solution of differential equations which contain the Laplace term. The main idea of the method is to treat all the terms except the Laplace term as a inhomogeneity and to approximate these inhomogeneities using the radial basis functions. Gümğüm and Tezer-Sezgin used DRBEM for the solution of the mixed convection of nanofluids in [10]. In this study, implicit Euler scheme was used for the approximation of the time derivatives and they discretized the boundary using linear boundary elements which is more complicated than the constant boundary elements.

In the present work, the influence of buoyancy force, heat source length and location, and nanoparticles on the fluid behavior is studied numerically. The stream function-vorticity-temperature (ψ - w - T) form of the governing equations are solved using DRBEM. First, before DRBEM is implemented, the vorticity transport and temperature equations are transformed to the inhomogeneous modified Helmholtz equations. These transformations are done by approximating the vorticity and temperature variables, which are located in the Laplace terms, with relaxation parameters and by approximating the time derivatives using forward difference approximations. Then, DRBEM is applied to the governing equations using the fundamental solution of Laplace equation for stream function equation, and using the fundamental solution of modified Helmholtz equations for vorticity transform and temperature equations. By using this way, more information is used from the original governing equations. Also, approximating the time derivatives at the beginning of the solution procedure one can eliminate the need of extra time integration scheme in DRBEM and stability analysis. Selecting appropriate relaxation parameters allows us to use large time steps, in this way a small number of iteration is enough to obtain good results. The numerical results are given for all physical parameters using the tables and graphs and comparing with the studies available in the literature.

NOMENCLATURE

B	heat source length
D	heat source location
f, \tilde{f}	radial basis functions for Poisson and modified Helmholtz equations
F, \tilde{F}	coordinate matrices for Poisson and modified Helmholtz equations
g	gravitational acceleration
H, G	BEM matrices for Poisson equation
H', G', H'', G''	BEM matrices for modified Helmholtz equations
k	thermal conductivity
L	length of the cavity
N_B, N_I	the number of boundary elements and internal nodes
p	pressure
Pr	Prandtl number
r	distance between source and field points
Ra	Rayleigh number
Re	Reynolds number
q''	heat generation per area
T	temperature
T_c	cold temperature
u, v	components of fluid velocity
u^*, q^*	fundamental solution and its normal derivative
\hat{u}, \hat{q}	particular solution and its normal derivative
w	vorticity

Greek symbols

$\alpha_1, \alpha_2, \alpha_3$	unknown coefficients
α	thermal diffusivity
β	thermal expansion coefficient
Γ	boundary of the domain
ΔT	reference temperature difference
Δt	time step
θ_w, θ_T	relaxation parameters
λ_w, λ_T	wave numbers
ν	kinematic viscosity
ρ	density
$(\rho\beta)$	thermal expansion coefficient of nanofluid
(ρC_p)	heat capacitance of nanofluid
ϕ	solid volume fraction
Ω	two-dimensional domain

Superscripts

'	dimensional parameters
(m)	time level

Subscripts

s	solid
f	fluid
nf	nanofluid

2. Governing equations

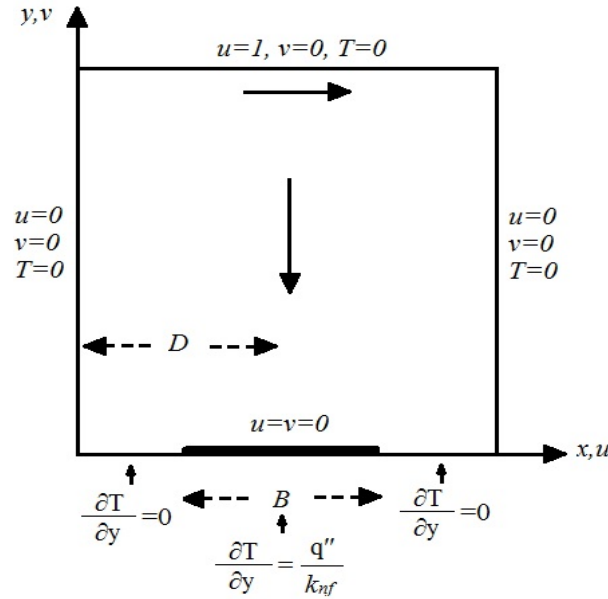


Figure 1. Domain of the problem.

The geometrical representation of the present problem defined in a square cavity with a heat source which is located on a part of the bottom wall is shown Figure (1). The heat source length and location are changed taking different values of B and D , respectively. The length of the heat source takes the shortest value at $B = 0.2$ whereas it takes the longest value at $B = 0.8$. Values of $D < 0.5$ indicate that the heat source is close to the left wall while $D > 0.5$ indicate that the heat source is close to the right wall. The top, left and right walls are maintained at constant cold temperatures (T_c). The bottom wall is kept as adiabatic both on the heat source and other parts of the boundary. The no-slip boundary conditions are imposed on all segments of the boundary with the exception of the upper wall, which is assumed to move from left to right with constant velocity $U_0 = 1$. Two-dimensional square cavity is filled with Cu -water nanofluid and the solid spherical nanoparticles are in the thermal equilibrium. The thermo-physical properties of the base fluid (water) and nanoparticles (Cu) and nanofluid are given in [14]. The non-dimensional governing equations for the unsteady, laminar natural convection flow of Newtonian and incompressible nanofluid can be written velocity (u, v), pressure (p) and temperature (T) form as [14]

$$\frac{\partial u}{\partial x} + \frac{\partial v}{\partial y} = 0, \tag{2.1}$$

$$\frac{\partial u}{\partial t} + u \frac{\partial u}{\partial x} + v \frac{\partial u}{\partial y} = -\frac{\partial p}{\partial x} + \frac{1}{Re} \frac{\rho_f}{\rho_{nf}} \frac{1}{(1-\phi)^{2.5}} \left[\frac{\partial^2 u}{\partial x^2} + \frac{\partial^2 u}{\partial y^2} \right], \tag{2.2}$$

$$\frac{\partial v}{\partial t} + u \frac{\partial v}{\partial x} + v \frac{\partial v}{\partial y} = -\frac{\partial p}{\partial y} + \frac{1}{Re} \frac{\rho_f}{\rho_{nf}} \frac{1}{(1-\phi)^{2.5}} \left[\frac{\partial^2 v}{\partial x^2} + \frac{\partial^2 v}{\partial y^2} \right] + \frac{(\rho\beta)_{nf}}{\rho_{nf}\beta_f} \frac{RaPr}{Re^2} T, \tag{2.3}$$

$$\frac{\partial T}{\partial t} + u \frac{\partial T}{\partial x} + v \frac{\partial T}{\partial y} = \frac{\alpha_{nf}}{\alpha_f} \frac{1}{RePr} \left[\frac{\partial^2 T}{\partial x^2} + \frac{\partial^2 T}{\partial y^2} \right] \tag{2.4}$$

with the non-dimensional parameters

$$x = \frac{x'}{L}, \quad y = \frac{y'}{L}, \quad u = \frac{u'}{U_0}, \quad v = \frac{v'}{U_0}, \quad T = \frac{T' - T_c}{\Delta T}, \quad p = \frac{p'}{\rho_{nf} U_0^2},$$

$$\Delta T = \frac{q'' L}{k_f}, \quad Ra = \frac{g \beta_f L^3 \Delta T}{\nu_f \alpha_f}, \quad Re = \frac{\rho_f U_0 L}{\mu_f}, \quad Pr = \frac{\nu_f}{\alpha_f}$$
(2.5)

where L , g , ΔT , q'' and ν are the length of the cavity, gravitational acceleration, reference temperature difference, heat generation per area and kinematic viscosity, respectively. The parameters with primes represent the dimensional parameters. Also, Re is the Reynolds number, Ra is the Rayleigh number and Pr is the Prandtl number. The Reynolds number is the ratio of inertia forces to viscous forces which is used to determine whether the characteristic behavior of fluid is laminar ($Re < 2000$) or turbulent ($Re > 4000$). In the fluids two different heat transfer mechanism can occur which are called convection and conduction. Rayleigh number is the property of a fluid that determines what kind of heat transfer occur throughout the fluid. Prandtl number is a fluid property which is the ratio between the fluid viscosity and thermal diffusivity and it does not contain any length and velocity scales. So, each fluid has different Prandtl number ($Pr \ll 1$ for liquid metals, $Pr < 1$ gases, $Pr > 1$ for light liquids, very large values for oils). The Prandtl number of water at $19.5^\circ C$ is 6.2 and this value is used in all analysis through in this study.

The properties of the base fluid and the solid particles, volume fraction of the solid particles and particles shape affect the thermo physical properties of the nanofluids. In equations (2.1)-(2.5), the parameters ρ_{nf} , $(\rho\beta)_{nf}$ and α_{nf} denote the effective density, thermal expansion coefficient of nanofluid and thermal diffusivity of nanofluid, respectively, and they can be determined by [14],

$$\rho_{nf} = (1 - \phi)\rho_f + \phi\rho_s, \quad (\rho\beta)_{nf} = (1 - \phi)(\rho\beta)_f + \phi(\rho\beta)_s,$$

$$\frac{k_{nf}}{k_f} = \frac{k_s + 2k_f - 2\phi(k_f - k_s)}{k_s + 2k_f + \phi(k_f - k_s)}, \quad (\rho C_p)_{nf} = (1 - \phi)(\rho C_p)_f + \phi(\rho C_p)_s,$$
(2.6)

$$\alpha_{nf} = \frac{k_{nf}}{(\rho C_p)_{nf}}$$

where, ρ is the density, ϕ is the solid volume fraction with the definition

$$\phi = \frac{\text{volume of the particle}}{\text{total volume of the nanofluid}},$$

β is the thermal expansion coefficient, $(\rho C_p)_{nf}$ is the heat capacitance of nanofluid, k is the thermal conductivity. The ratio for thermal conductivity is called the Maxwell-Garnett's model for spherical nanoparticles. The notations 's', 'f' and 'nf' represent the value of parameters for solid, fluid and nanofluid, respectively.

Using the definitions of velocity components (u and v) and vorticity (w) as

$$u = \frac{\partial\psi}{\partial y}, \quad v = -\frac{\partial\psi}{\partial x}, \quad w = \frac{\partial v}{\partial x} - \frac{\partial u}{\partial y}$$
(2.7)

the governing equations (2.1)-(2.4) can be written as

$$\nabla^2\psi = -w,$$
(2.8)

$$\frac{1}{Re} \frac{\rho_f}{\rho_{nf}} \frac{1}{(1 - \phi)^{2.5}} \nabla^2 w = \frac{\partial w}{\partial t} + u \frac{\partial w}{\partial x} + v \frac{\partial w}{\partial y} - \frac{Ra Pr}{Re^2} \frac{(\rho\beta)_{nf}}{\rho_{nf} \beta_f} \frac{\partial T}{\partial x},$$
(2.9)

$$\frac{1}{Pr Re} \frac{\alpha_{nf}}{\alpha_f} \nabla^2 T = \frac{\partial T}{\partial t} + u \frac{\partial T}{\partial x} + v \frac{\partial T}{\partial y}.$$
(2.10)

The time derivatives in Equations (2.9) and (2.10) are approximated with the forward finite difference approximations

$$\frac{\partial w}{\partial t} = \frac{w^{(m+1)} - w^{(m)}}{\Delta t} \quad \text{and} \quad \frac{\partial T}{\partial t} = \frac{T^{(m+1)} - T^{(m)}}{\Delta t}, \quad (2.11)$$

where $w^{(m)} = w(x, y, t_m)$, $T^{(m)} = T(x, y, t_m)$, $t_m = m\Delta t$ and Δt is the time step. w and T at the left hand sides of the equations (2.9) and (2.10) are expanded at the two successive time levels with relaxation parameters θ_w and θ_T as

$$w^{(m+1)} = \theta_w w^{(m+1)} + (1 - \theta_w)w^{(m)} \quad \text{and} \quad T^{(m+1)} = \theta_T T^{(m+1)} + (1 - \theta_T)T^{(m)}. \quad (2.12)$$

Inserting the approximations (2.11) and (2.12) into the Equations (2.9) and (2.10) the iterative form of the governing equations are constructed as

$$\begin{aligned} \nabla^2 \psi^{(m+1)} &= -w^{(m)}, \\ \nabla^2 w^{(m+1)} - \lambda_w^2 w^{(m+1)} &= \frac{(\theta_w - 1)}{\theta_w} \nabla^2 w^{(m)} - \lambda_w^2 w^{(m)} \\ &+ Re \frac{\rho_{nf}(1 - \phi)^{2.5}}{\rho_f \theta_w} \left(\frac{\partial \psi^{(m+1)}}{\partial y} \frac{\partial w^{(m)}}{\partial x} - \frac{\partial \psi^{(m+1)}}{\partial x} \frac{\partial w^{(m)}}{\partial y} \right) \\ &- \frac{RaPr}{Re} \frac{(\rho\beta)_{nf}(1 - \phi)^{2.5}}{\beta_f \rho_f \theta_w} \frac{\partial T^{(m)}}{\partial x}, \\ \nabla^2 T^{(m+1)} - \lambda_T^2 T^{(m+1)} &= \frac{(\theta_T - 1)}{\theta_T} \nabla^2 T^{(m)} - \lambda_T^2 T^{(m)} \\ &+ PrRe \frac{\alpha_f}{\alpha_{nf} \theta_T} \left(\frac{\partial \psi^{(m+1)}}{\partial y} \frac{\partial T^{(m)}}{\partial x} - \frac{\partial \psi^{(m+1)}}{\partial x} \frac{\partial T^{(m)}}{\partial y} \right) \end{aligned} \quad (2.13)$$

where $\lambda_w^2 = Re \frac{\rho_{nf}(1 - \phi)^{2.5}}{\rho_f \Delta t \theta_w}$ and $\lambda_T^2 = PrRe \frac{\alpha_f}{\alpha_{nf} \Delta t \theta_T}$, and m indicates iteration number.

3. DRBEM formulation

The aim of this section to find a simple way to solve the governing equations (2.13) without computing any domain integral. Therefore, the governing equations (2.13) of the problem are transformed into boundary integral equations using the DRBEM. In the solution procedure, all the terms except the Laplace and modified Helmholtz equations are considered as inhomogeneity [19], [2]. Let, \hat{u}_i 's ($i = 1, 2, 3$) be particular solutions

which satisfy the following equations

$$\begin{aligned}
 \nabla^2 \hat{u}_1 &= -w^{(m)}, \\
 \nabla^2 \hat{u}_2 - \lambda_w^2 \hat{u}_2 &= \frac{(\theta_w - 1)}{\theta_w} \nabla^2 w^{(m)} - \lambda_w^2 w^{(m)} \\
 &\quad + Re \frac{\rho_{nf}(1 - \phi)^{2.5}}{\rho_f \theta_w} \left(\frac{\partial \psi^{(m+1)}}{\partial y} \frac{\partial w^{(m)}}{\partial x} - \frac{\partial \psi^{(m+1)}}{\partial x} \frac{\partial w^{(m)}}{\partial y} \right) \\
 &\quad - \frac{RaPr (\rho\beta)_{nf}(1 - \phi)^{2.5}}{Re \beta_f \rho_f \theta_w} \frac{\partial T^{(m)}}{\partial x}, \\
 \nabla^2 \hat{u}_3 - \lambda_T^2 \hat{u}_3 &= \frac{(\theta_T - 1)}{\theta_T} \nabla^2 T^{(m)} - \lambda_T^2 T^{(m)} \\
 &\quad + PrRe \frac{\alpha_f}{\alpha_{nf} \theta_T} \left(\frac{\partial \psi^{(m+1)}}{\partial y} \frac{\partial T^{(m)}}{\partial x} - \frac{\partial \psi^{(m+1)}}{\partial x} \frac{\partial T^{(m)}}{\partial y} \right).
 \end{aligned} \tag{3.1}$$

In the DRBEM idea, a series of particular solutions $\hat{u}_{i,j}$'s ($i = 1, 2, 3$) are used instead of a single \hat{u}_i , ($i = 1, 2, 3$) function and inhomogeneities are approximated using the radial basis functions f_j 's ($f_j = 1 + r_j$) and \tilde{f}_j 's ($\tilde{f}_j = r_j^2 \log r_j$) as

$$\begin{aligned}
 \sum_{j=1}^{N_B+N_I} \alpha_{1j} f_j(x, y) &= -w^{(m)}, \\
 \sum_{j=1}^{N_B+N_I} \alpha_{2j}(t) \tilde{f}_j(x, y) &= \frac{(\theta_w - 1)}{\theta_w} \nabla^2 w^{(m)} - \lambda_w^2 w^{(m)} \\
 &\quad + Re \frac{\rho_{nf}(1 - \phi)^{2.5}}{\rho_f \theta_w} \left(\frac{\partial \psi^{(m+1)}}{\partial y} \frac{\partial w^{(m)}}{\partial x} - \frac{\partial \psi^{(m+1)}}{\partial x} \frac{\partial w^{(m)}}{\partial y} \right) \\
 &\quad - \frac{RaPr (\rho\beta)_{nf}(1 - \phi)^{2.5}}{Re \beta_f \rho_f \theta_w} \frac{\partial T^{(m)}}{\partial x}, \\
 \sum_{j=1}^{N_B+N_I} \alpha_{3j}(t) \tilde{f}_j(x, y) &= \frac{(\theta_T - 1)}{\theta_T} \nabla^2 T^{(m)} - \lambda_T^2 T^{(m)} \\
 &\quad + PrRe \frac{\alpha_f}{\alpha_{nf} \theta_T} \left(\frac{\partial \psi^{(m+1)}}{\partial y} \frac{\partial T^{(m)}}{\partial x} - \frac{\partial \psi^{(m+1)}}{\partial x} \frac{\partial T^{(m)}}{\partial y} \right)
 \end{aligned} \tag{3.2}$$

where N_B is the number of the constant boundary elements and N_I is the number of interior points. f_j 's are linked with the particular solutions \hat{u}_{1j} to the equations $\nabla^2 \hat{u}_{1j} = f_j$, and \tilde{f}_j 's are linked with the particular solutions \hat{u}_{2j} and \hat{u}_{3j} to the equations $(\nabla^2 - \lambda_w^2) \hat{u}_{2j} = \tilde{f}_j$ and $(\nabla^2 - \lambda_T^2) \hat{u}_{3j} = \tilde{f}_j$, respectively. The coefficients α_{1j} are unknown constants whereas α_{2j} and α_{3j} are initially unknown time dependent coefficients.

After substituting the approximations for f_j and \tilde{f}_j into the equation (3.2) new approximations are obtained as

$$\begin{aligned}
 & \sum_{j=1}^{N_B+N_I} \alpha_{1j} \nabla^2 \hat{u}_{1j} = -w^{(m)}, \\
 & \sum_{j=1}^{N_B+N_I} \alpha_{2j}(t) (\nabla^2 - \lambda_w^2) \hat{u}_{2j} = \frac{(\theta_w - 1)}{\theta_w} \nabla^2 w^{(m)} - \lambda_w^2 w^{(m)} \\
 & + Re \frac{\rho_{nf}(1 - \phi)^{2.5}}{\rho_f \theta_w} \left(\frac{\partial \psi^{(m+1)}}{\partial y} \frac{\partial w^{(m)}}{\partial x} - \frac{\partial \psi^{(m+1)}}{\partial x} \frac{\partial w^{(m)}}{\partial y} \right) \\
 & - \frac{RaPr}{Re} \frac{(\rho\beta)_{nf}(1 - \phi)^{2.5}}{\beta_f \rho_f \theta_w} \frac{\partial T^{(m)}}{\partial x}, \\
 & \sum_{j=1}^{N_B+N_I} \alpha_{3j} ((\nabla^2 - \lambda_T^2) \hat{u}_{3j} t) = \frac{(\theta_T - 1)}{\theta_T} \nabla^2 T^{(m)} - \lambda_T^2 T^{(m)} \\
 & + PrRe \frac{\alpha_f}{\alpha_{nf} \theta_T} \left(\frac{\partial \psi^{(m+1)}}{\partial y} \frac{\partial T^{(m)}}{\partial x} - \frac{\partial \psi^{(m+1)}}{\partial x} \frac{\partial T^{(m)}}{\partial y} \right).
 \end{aligned} \tag{3.3}$$

Substituting the equation (3.3) into (2.13)

$$\begin{aligned}
 \nabla^2 \psi^{(m+1)} &= \sum_{j=1}^{N_B+N_I} \alpha_{1j} \nabla^2 \hat{u}_{1j}, \\
 \nabla^2 w^{(m+1)} - \lambda_w^2 w^{(m+1)} &= \sum_{j=1}^{N_B+N_I} \alpha_{2j}(t) (\nabla^2 \hat{u}_{2j} - \lambda_w^2 \hat{u}_{2j}), \\
 \nabla^2 T^{(m+1)} - \lambda_T^2 T^{(m+1)} &= \sum_{j=1}^{N_B+N_I} \alpha_{3j}(t) (\nabla^2 \hat{u}_{3j} - \lambda_T^2 \hat{u}_{3j}).
 \end{aligned} \tag{3.4}$$

Thus, Laplace and modified Helmholtz operators occur to be in both sides. Then, equations are weighted with the corresponding fundamental solutions and are integrated over the domain as in [19], [2]

$$\begin{aligned}
 \int_{\Omega} (\nabla^2 \psi^{(m+1)}) u_1^* d\Omega &= \sum_{j=1}^{N_B+N_I} \alpha_{1j} \int_{\Omega} (\nabla^2 \hat{u}_{1j}) u_1^* d\Omega, \\
 \int_{\Omega} (\nabla^2 w^{(m+1)} - \lambda_w^2 w^{(m+1)}) u_2^* d\Omega &= \sum_{j=1}^{N_B+N_I} \alpha_{2j}(t) \int_{\Omega} (\nabla^2 \hat{u}_{2j} - \lambda_w^2 \hat{u}_{2j}) u_2^* d\Omega, \\
 \int_{\Omega} (\nabla^2 T^{(m+1)} - \lambda_T^2 T^{(m+1)}) u_3^* d\Omega &= \sum_{j=1}^{N_B+N_I} \alpha_{3j}(t) \int_{\Omega} (\nabla^2 \hat{u}_{3j} - \lambda_T^2 \hat{u}_{3j}) u_3^* d\Omega,
 \end{aligned} \tag{3.5}$$

where $u_1^* = \frac{1}{2\pi} \ln(r)$ (fundamental solution of Laplace equation), $u_2^* = \frac{1}{2\pi} K_0(\lambda_w r)$ and $u_3^* = \frac{1}{2\pi} K_0(\lambda_T r)$ (fundamental solutions of modified Helmholtz equations). $K_0(\lambda_w r)$ and $K_0(\lambda_T r)$ are second kind modified Bessel functions of order zero where r is the distance between the source and the field points. Then, after applying Green's second identity

following integral equations can be obtained for each source point i

$$\begin{aligned}
 c_i \psi_i^{(m+1)} + \int_{\Gamma} \left(q_1^* \psi^{(m+1)} - u_1^* \frac{\partial \psi^{(m+1)}}{\partial n} \right) d\Gamma = \\
 \sum_{j=1}^{N_B+N_I} \alpha_{1j} \left[c_i \hat{u}_{1ji} \int_{\Gamma} \left(q_1^* \hat{u}_{1j} - u_1^* \frac{\partial \hat{u}_{1j}}{\partial n} \right) d\Gamma \right], \\
 c_i w_i^{(m+1)} + \int_{\Gamma} \left(q_2^* w^{(m+1)} - u_2^* \frac{\partial w^{(m+1)}}{\partial n} \right) d\Gamma = \\
 \sum_{j=1}^{N_B+N_I} \alpha_{2j}(t) \left[c_i \hat{u}_{2ji} \int_{\Gamma} \left(q_2^* \hat{u}_{2j} - u_2^* \frac{\partial \hat{u}_{2j}}{\partial n} \right) d\Gamma \right], \\
 c_i T_i^{(m+1)} + \int_{\Gamma} \left(q_3^* T^{(m+1)} - u_3^* \frac{\partial T^{(m+1)}}{\partial n} \right) d\Gamma = \\
 \sum_{j=1}^{N_B+N_I} \alpha_{3j}(t) \left[c_i \hat{u}_{3ji} \int_{\Gamma} \left(q_3^* \hat{u}_{3j} - u_3^* \frac{\partial \hat{u}_{3j}}{\partial n} \right) d\Gamma \right]
 \end{aligned} \tag{3.6}$$

where $q_1^* = \frac{\partial u_1^*}{\partial n}$, $q_2^* = \frac{\partial u_2^*}{\partial n}$, $q_3^* = \frac{\partial u_3^*}{\partial n}$, and the constant c_i is $c_i = \gamma_i/2\pi$, γ_i is the internal angle at the point i , Γ is the boundary of the domain Ω . The derivation of particular solutions and their normal derivatives is given in [2] and [19]. After discretizing the boundary using N_B constant elements and taking the N_I interior nodes for the solution of unknowns ψ , w , T and their normal derivatives we get the matrix-vector form of the governing equations as

$$\begin{aligned}
 \mathbf{H}\boldsymbol{\psi}^{(m+1)} - \mathbf{G} \frac{\partial \boldsymbol{\psi}^{(m+1)}}{\partial n} &= \left(\mathbf{H}\widehat{\mathbf{U}} - \mathbf{G}\widehat{\mathbf{Q}} \right) \boldsymbol{\alpha}_1, \\
 \mathbf{H}'\mathbf{w}^{(m+1)} + \mathbf{G}' \frac{\partial \mathbf{w}^{(m+1)}}{\partial n} &= \left(\mathbf{H}'\widehat{\mathbf{U}}' + \mathbf{G}'\widehat{\mathbf{Q}}' \right) \boldsymbol{\alpha}_2, \\
 \mathbf{H}''\mathbf{T}^{(m+1)} + \mathbf{G}'' \frac{\partial \mathbf{T}^{(m+1)}}{\partial n} &= \left(\mathbf{H}''\widehat{\mathbf{U}}'' + \mathbf{G}''\widehat{\mathbf{Q}}'' \right) \boldsymbol{\alpha}_3
 \end{aligned} \tag{3.7}$$

where

$$\begin{aligned}
 \boldsymbol{\alpha}_1 &= \mathbf{F}^{-1} \left\{ -\mathbf{w}^{(m)} \right\}, \\
 \boldsymbol{\alpha}_2 &= \tilde{\mathbf{F}}^{-1} \frac{(\theta_w - 1)}{\theta_w} \nabla^2 \mathbf{w}^{(m)} - \lambda_w^2 \mathbf{w}^{(m)} \\
 &+ Re \frac{\rho_{nf}(1-\phi)^{2.5}}{\rho_f \theta_w} \left(\frac{\partial \psi^{(m+1)}}{\partial y} \frac{\partial w^{(m)}}{\partial x} - \frac{\partial \psi^{(m+1)}}{\partial x} \frac{\partial w^{(m)}}{\partial y} \right) \\
 &- \frac{RaPr(\rho\beta)_{nf}(1-\phi)^{2.5}}{Re \beta_f \rho_f \theta_w} \frac{\partial T^{(m)}}{\partial x}, \\
 \boldsymbol{\alpha}_3 &= \frac{(\theta_T - 1)}{\theta_T} \nabla^2 T^{(m)} - \lambda_T^2 T^{(m)} \\
 &+ PrRe \frac{\alpha_f}{\alpha_{nf} \theta_T} \left(\frac{\partial \psi^{(m+1)}}{\partial y} \frac{\partial T^{(m)}}{\partial x} - \frac{\partial \psi^{(m+1)}}{\partial x} \frac{\partial T^{(m)}}{\partial y} \right).
 \end{aligned} \tag{3.8}$$

Here \mathbf{F}^{-1} and $\tilde{\mathbf{F}}^{-1}$ contain the coordinate functions f_j and \tilde{f}_j 's as columns for $i = 1, 2, \dots, N_B + N_I$, respectively. The dimensions of the matrices and vectors are expanded taking into account N_I interior nodes. Therefore, their dimensions in these discretized systems are $(N_B + N_I) \times (N_B + N_I)$ and $(N_B + N_I) \times 1$, respectively. The matrices $\hat{\mathbf{U}}, \hat{\mathbf{U}}', \hat{\mathbf{U}}'', \hat{\mathbf{Q}}, \hat{\mathbf{Q}}'$ and $\hat{\mathbf{Q}}''$ are constructed by taking each of the vectors $\hat{\mathbf{u}}_{1j}, \hat{\mathbf{u}}_{2j}, \hat{\mathbf{u}}_{3j}, \hat{\mathbf{q}}_{1j}, \hat{\mathbf{q}}_{2j}$ and $\hat{\mathbf{q}}_{3j}$ as columns for $i = 1, \dots, N_B + N_I$, respectively. The components of the coefficient matrices are [3, 6]

$$\begin{aligned} H_{ij} &= c_i \delta_{ij} + \frac{1}{2\pi} \int_{\Gamma_j} \frac{\partial}{\partial n} \left(\ln \left(\frac{1}{r} \right) \right) d\Gamma_j, & G_{ij} &= \frac{1}{2\pi} \int_{\Gamma_j} \ln \left(\frac{1}{r} \right) d\Gamma_j, \\ H_{ij}' &= c_i \delta_{ij} + \frac{1}{2\pi} \int_{\Gamma_j} \frac{\partial K_0(\lambda_w r_i)}{\partial n} d\Gamma, & G_{ij}' &= -\frac{1}{2\pi} \int_{\Gamma_j} K_0(\lambda_w r_i) d\Gamma, \\ H_{ij}'' &= c_i \delta_{ij} + \frac{1}{2\pi} \int_{\Gamma_j} \frac{\partial K_0(\lambda_T r_i)}{\partial n} d\Gamma, & G_{ij}'' &= -\frac{1}{2\pi} \int_{\Gamma_j} K_0(\lambda_T r_i) d\Gamma. \end{aligned} \quad (3.9)$$

Here δ_{ij} , Γ_j and r are the Kronecker delta function, the boundary of the j -th element and the length of the distance vector from boundary point i to j .

In the computations, first and second derivatives of all unknowns are approximated using the DRBEM idea as

$$\frac{\partial \mathbf{Z}}{\partial x} = \frac{\partial \tilde{\mathbf{F}}}{\partial x} \tilde{\mathbf{F}}^{-1} \mathbf{Z}, \quad \frac{\partial \mathbf{Z}}{\partial y} = \frac{\partial \tilde{\mathbf{F}}}{\partial y} \tilde{\mathbf{F}}^{-1} \mathbf{Z} \quad (3.10)$$

where Z is used for the unknowns $\psi^{(m+1)}$, $\mathbf{w}^{(m)}$, $\mathbf{T}^{(m)}$, $\frac{\partial \psi^{(m+1)}}{\partial x}$ and $\frac{\partial \psi^{(m+1)}}{\partial y}$. The imposed vorticity boundary conditions are also obtained using the DRBEM idea as

$$w = - \left[\frac{\partial \tilde{\mathbf{F}}}{\partial x} \tilde{\mathbf{F}}^{-1} \left(\frac{\partial \tilde{\mathbf{F}}}{\partial x} \tilde{\mathbf{F}}^{-1} \psi^{(m+1)} \right) + \frac{\partial \tilde{\mathbf{F}}}{\partial y} \tilde{\mathbf{F}}^{-1} \left(\frac{\partial \tilde{\mathbf{F}}}{\partial y} \tilde{\mathbf{F}}^{-1} \psi^{(m+1)} \right) \right]. \quad (3.11)$$

The solutions can be obtained by solving the system of equations (3.7) and (3.8), iteratively, after inserting the initial and boundary conditions.

4. Numerical results

In this part of the study, two-dimensional unsteady mixed convection flow of Cu -water based nanofluids depicted in Figure (1) is numerically discretized using the DRBEM. In the stream function-vorticity-temperature form of the equations (2.8)-(2.10) are used as governing equations. The unknown vorticity boundary conditions are obtained using the definition of vorticity in (2.7) with the DRBEM coordinate matrix. Due to the no-slip boundary conditions of velocities, stream function boundary conditions are taken zero at all sides of the cavity. The dimensionless form of the temperature boundary conditions are taken as

$$\begin{aligned} T &= 0, & x &= 0, & 0 &\leq y \leq 1 \\ T &= 0, & x &= 1, & 0 &\leq y \leq 1 \\ T &= 0, & y &= 1, & 0 &\leq x \leq 1 \\ \frac{\partial T}{\partial y} &= 0, & y &= 0, & 0 &\leq x \leq (D - 0.5B) \\ \frac{\partial T}{\partial y} &= \frac{k_f}{k_{nf}}, & y &= 0, & (D - 0.5B) &\leq x \leq (D + 0.5B) \\ \frac{\partial T}{\partial y} &= 0, & y &= 0, & (D + 0.5B) &\leq x \leq 1. \end{aligned} \quad (4.1)$$

The local Nusselt number of the nanofluid along the heat source surface can be expressed as

$$Nu_s(x) = \frac{1}{T_s(x)} \tag{4.2}$$

where $T_s(x)$ is the temperature of the heat source. The average Nusselt number is calculated by integrating local Nusselt number over the heat source

$$Nu_m = \frac{1}{B} \int_{D-0.5B}^{D+0.5B} Nu_s(x). \tag{4.3}$$

Numerical procedure is used to carry out for the physical parameters Ra , Re , ϕ , B and D to show their influence on the streamlines, vorticity and temperature contourlines. To obtain steady state results using small number of iterations, the relaxation parameters are taken $\theta_w = \theta_T = 0.9$ [3]. The stopping criteria for the iterative procedures is taken as 10^{-5} .

Forward finite difference scheme is the simplest time derivative discretization method. But, since it is explicit method, the stability problems are usually expected. So, the choice of Δt is the important point for the stability of this numerical method. Here, the choice of Δt is closely related with the behavior of $K_0(x)$ due to its location in the relation parameters $\lambda_w^2 = Re \frac{\rho_{nf}(1-\phi)^{2.5}}{\rho_f \Delta t \theta_w}$ and $\lambda_T^2 = Pr Re \frac{\alpha_f}{\alpha_{nf} \Delta t \theta_T}$. The $K_0(x) \rightarrow \infty$ (as $x \rightarrow \infty$) behavior is prevented by taking not too small time step size. In each analysis the solutions are kept stable by choosing suitable Δt depending on the values of other parameters. In all computations too small step size is not needed and it takes the values between 0.1 to 0.002.

Grid dependency is tested using several number of the boundary elements and the results are given for $Ra = 10^4$, $Re = 10$, $\phi = 0.1$, $B = 0.4$ and $D = 0.5$. in Figure (2). From the figure, $N_B = 200$ constant boundary elements satisfy the grid independence.

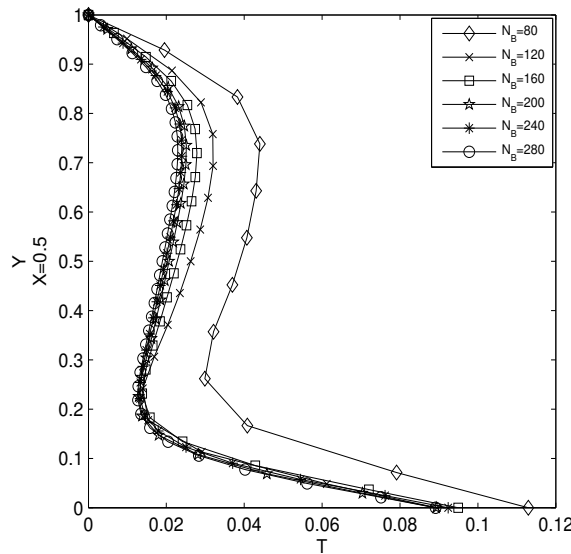


Figure 2. Grid independency analysis for $Ra = 10^4$, $Re = 10$, $\phi = 0.1$, $B = 0.4$ and $D = 0.5$.

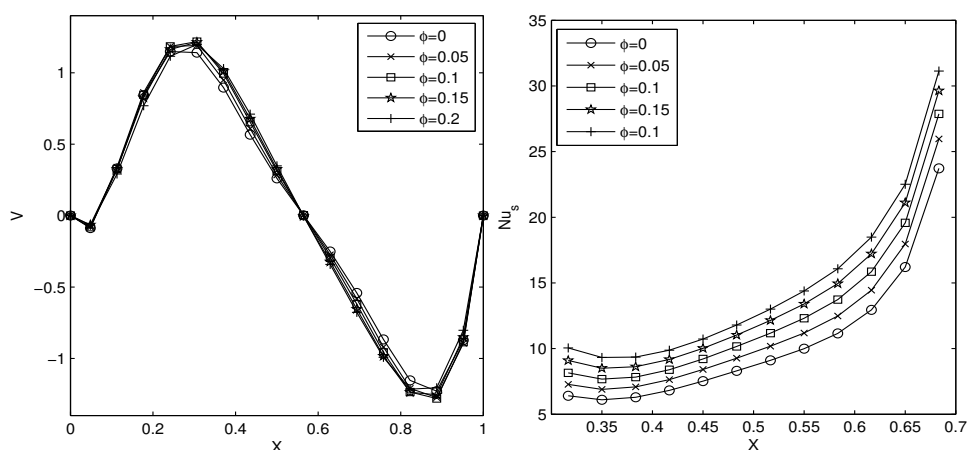


Figure 3. Code validation for $Ra = 10^4$, $Re = 10$, $B = 0.4$ and $D = 0.5$.

Code validation is done using the same parameter with [14] by drawing vertical velocity component at the mid section of the cavity and Nusselt number along the heat source, and results are given in Figure (3). In the computations the physical parameters are taken as $Ra = 10^4$, $Re = 10$, $B = 0.4$ and $D = 0.5$ whereas solid volume fraction is taken between 0 to 0.2. Obtained results are in good agreement with the solutions given in the work of [14].

Beside the adding nanoparticles with high thermal conductivity in a base fluid with low thermal conductivity, there are many factors to increase the effective thermal conductivity of nanofluids [12]. One of them is the solid volume fraction which is the ratio of volume of the particle and total volume of the nanofluid. The effect of solid volume fraction on the streamlines, vorticity and temperature at $Ra = 10^4$, $Re = 10$, $B = 0.4$ and $D = 0.5$ for Cu -water nanofluid is displayed in Figure (4). It is observed that the streamlines show a circular behavior and it takes the minimum value in the center of the cavity. This behavior is caused by the moving lid. The buoyancy forces caused by the temperature difference also assists this circular behavior. The fluid is heated by heater located at the bottom wall and other walls of the cavity are cooled. Thus, the density due to the temperature gradient near the bottom wall and top lid plays an important role in the emergence of the buoyancy forces. Because the density near the bottom wall is lower than the density near the top lid. Therefore, the lighter fluid moves from bottom wall towards the top lid and hence the circular behavior occur in the cavity. From the figure it can be concluded that, when ϕ increases, the magnitude of the streamlines decreases. Since the increasing value of solid volume fraction reduces the intensity of the buoyancy force, the flow intensity are effected, negatively. The vorticity contours are affected very little by the changing values of solid volume fraction and they show almost the similar profiles for all cases of solid volume fraction. But, the reduction of the intensity of buoyancy forces can be seen here, too. In the absence of the nanoparticle ($\phi = 0$), two central vortices occur in the center of the cavity and when solid volume fraction increases to 0.1 one of them is became disappear and then when it achieves to 0.2 they are vanished, completely. On the other hand, when $\phi = 0$ the temperature contourlines take place in the whole cavity but then an increase in ϕ to 0.2 leads the reduction of the fluid temperature and contourlines approach towards to the heater.

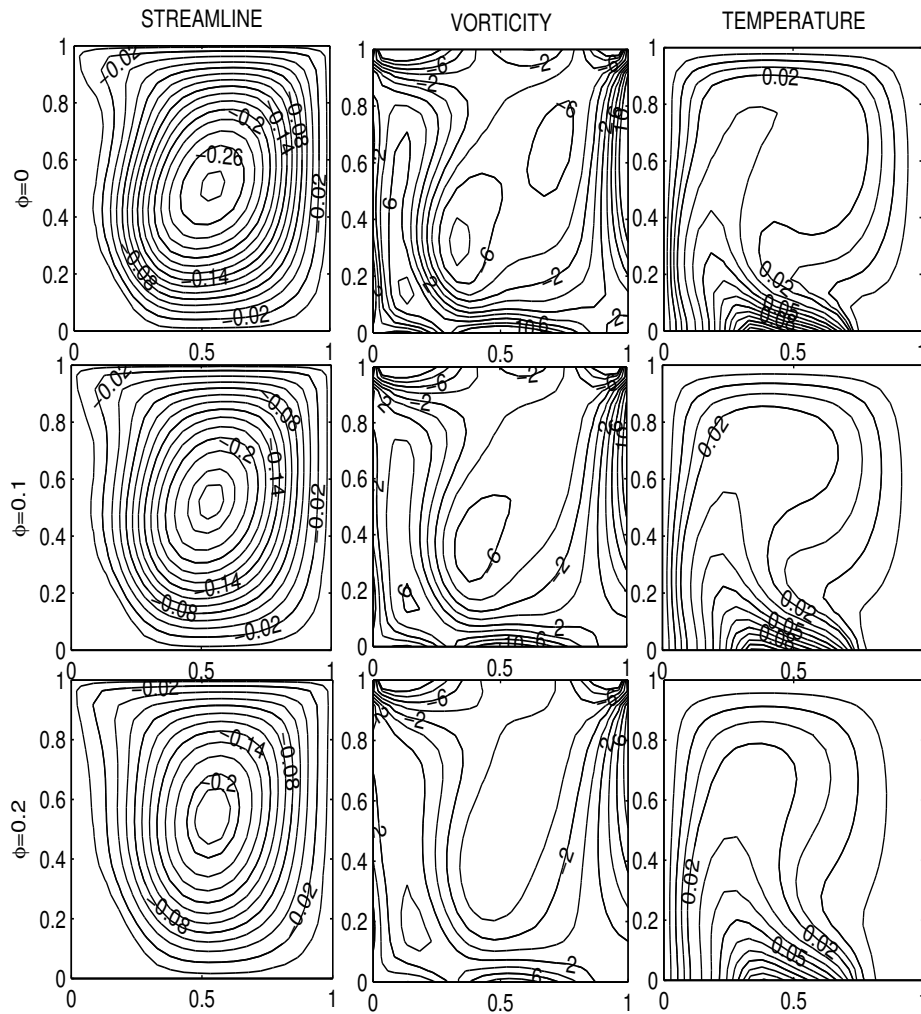


Figure 4. *Cu*-based nanofluid for several volume fraction when $Ra = 10^4$, $Re = 10$, $B = 0.4$ and $D = 0.5$.

Figure (5) displays the effect of heat source length on the fluid flow behavior by using several values of B . Results are given for heat source length ($B = 0.2, 0.4, 0.6, 0.8$) at $Ra = 10^4$, $Re = 10$, $\phi = 0.1$ and $D = 0.5$. The influence of the heat source length on the variables can be seen very clear. From the figures, it can be concluded that as the length of the heat source increases, the magnitude of the streamlines increases, the vorticity contourlines are distributed every side of the channel, and isotherms are more dense intensifies around the heat source and their intensity increases. All these behaviors are caused by the increasing value of the fluid temperature and increasing the flow intensity hence the increasing activity of the fluid motion. In other words, longer heat source increases the generation rates of the temperature.

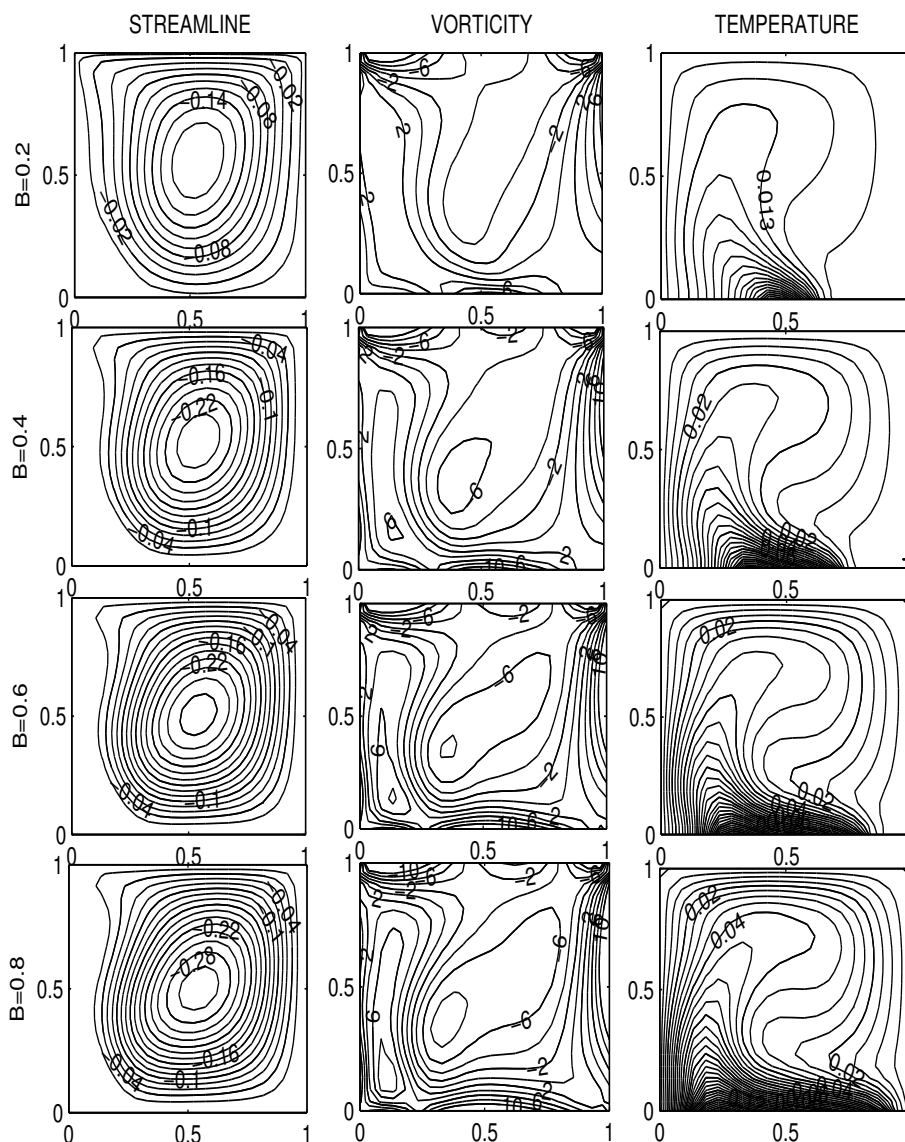


Figure 5. *Cu*-based nanofluid for several B when $Ra = 10^4$, $Re = 10$, $\phi = 0.1$ and $D = 0.5$.

Another analysis is done to show the effect of the heat source location and results are given in Figure (6). In the computations, different heat source locations ($D = 0.2, 0.4, 0.6, 0.8$) are tested by taking $Ra = 1.4 \times 10^4$, $Re = 10$, $\phi = 0.05$ and $B = 0.2$. From the figure it can be said that, the circular behavior of streamline occurs again but in this case their geometry changes depending on the location of the heat source. When the heat source is located in the middle of the bottom wall, one clockwise circular cell occur in the cavity. The same behavior occurs again as the heat source moves towards the left wall but their intensity decreases. However, when the heat source moves to the right side of the cavity which is the same direction with the moving lid, two circular vortex occur, one in the clockwise direction and the other in the opposite direction.

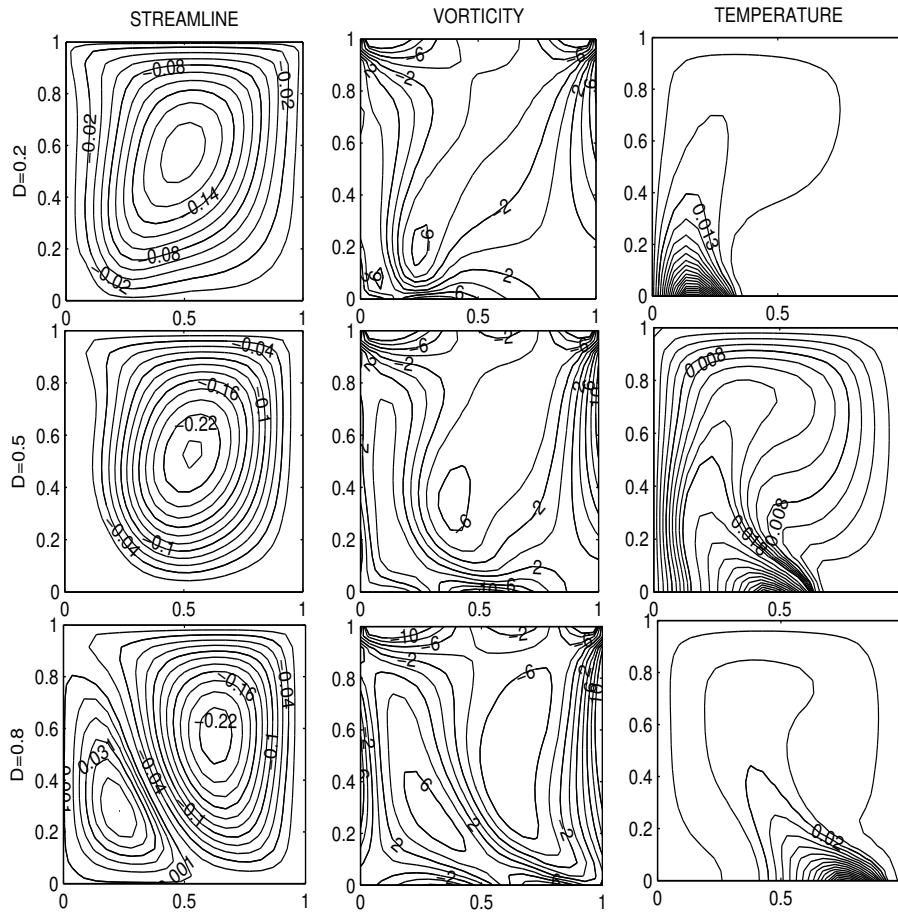


Figure 6. C_u -based nanofluid for several D when $Ra = 1.4 \times 10^4$, $Re = 10$, $\phi = 0.05$ and $B = 0.2$

Vorticity contour lines show the similar behavior with the streamlines which cover almost all parts of the cavity and form two vortex at the center. From the temperature contourlines, the location of the heat source can be seen easily since they follow the heat source movement. Although not as clear as the temperature contour lines, the movement of the heat source can also be monitored from the vorticity contour lines. These results show there is an important relation between the direction of the lid movement and the location of the heat source. Different situations create different results for the buoyancy forces where they may oppose or aid each other. When they moved the same direction the fluid buoyancy forces act together and hence the flow intensity increases. However, when they moved the reverse direction buoyancy forces oppose the each other and consequently the flow intensity decreases.

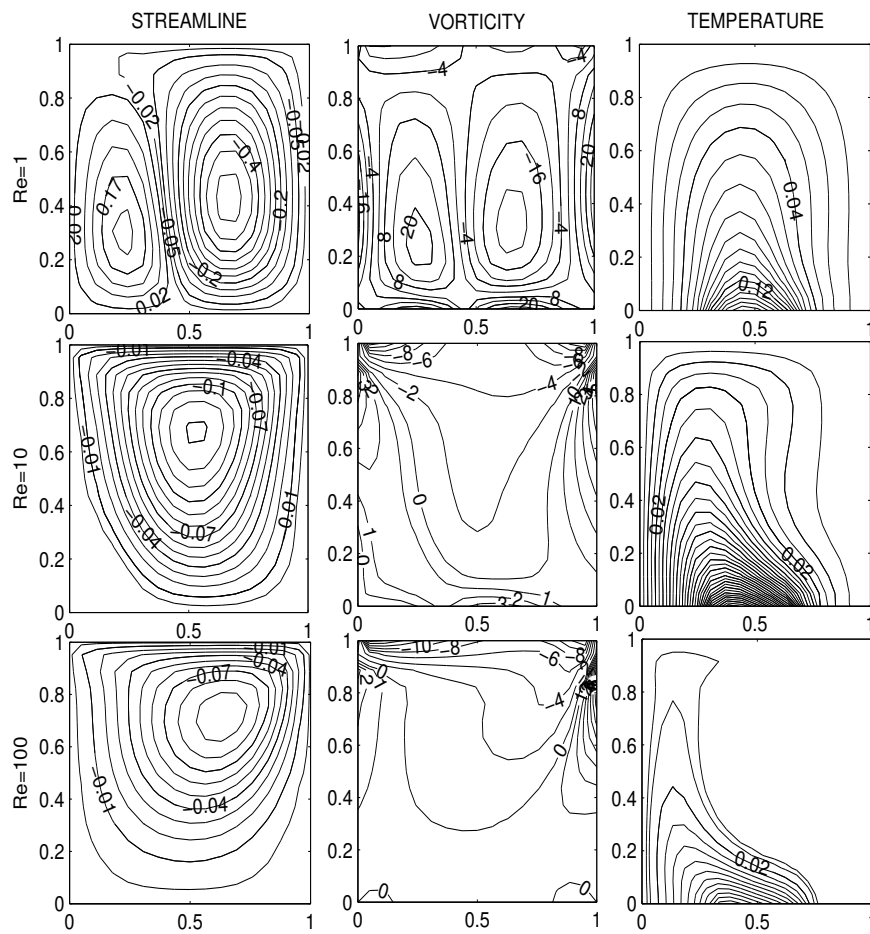


Figure 7. *Cu*-based nanofluid for several Re when $Ra = 10^3$, $\phi = 0.1$, $B = 0.4$ and $D = 0.5$

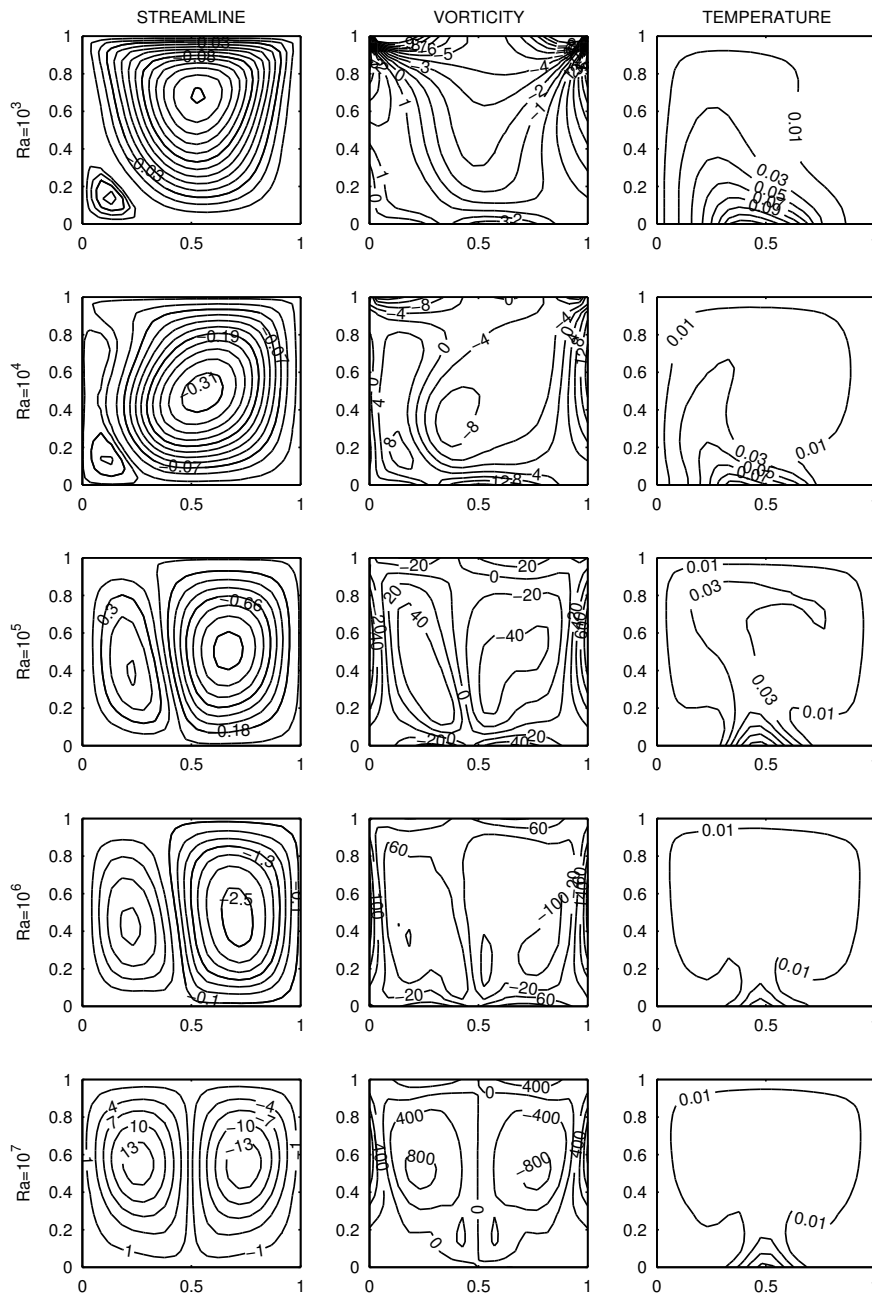


Figure 8. *Cu*-based nanofluid for several Ra when $Re = 10$, $\phi = 0.1$, $B = 0.4$ and $D = 0.5$

In this problem, both natural (due to the temperature difference) and forced (due to the moving lid as an external force) convection occur in the system so it is called mixed convection. The fluid behavior of dominating the forced convection can be analyzed by changing the Reynolds number. The effect of Reynolds number is investigated with

$Ra = 10^3$, $\phi = 0.1$, $B = 0.4$ and $D = 0.5$ for the values $Re < 100$ (laminar flow) and the results are depicted in Figure (7). For lower values of Re there is negligible lid-driven effect in the system and flow action occurs near the heat source. In this case heat transfer mechanism is conducted by natural convection. As Reynolds number increases, forced convection increases and it dominates the system. For $Re = 100$, the fluid motion occurs near the top lid by moving together with the lid. Because, as the Re increases the magnitude of the velocity components increase and turning points get closer to the top lid. Beside this, buoyancy forces caused by the temperature difference to become less influential relative to buoyancy forces caused by the moving lid. Hence the effect of the heat source on the streamlines is negligible. The increase in Reynolds number has similar effects on vorticity and temperature contours. Although the temperature contourlines are located central part of the cavity for $Re = 1$, they are located at the left side of the cavity as Reynolds number increases. For lower values of Reynolds number vorticity contour lines can be seen every side of the cavity, however, they move away from the center of the cavity towards the cavity walls as Re increases.

In the fluids two different heat transfer mechanism can occur which are called convection and conduction. The value of Rayleigh number determine the reason of heat transfer convection or conduction. Conduction occurs at low values of the Rayleigh number, $Ra < 10^3$, and convection occurs at Rayleigh numbers slightly exceeding the critical value of $Ra = 10^3$. If Ra takes the larger values then convection becomes chaotic. The effect of Rayleigh number on the fluid is given in Figure (8). In this analysis, the computations are done by taking $Re = 10$, $\phi = 0.1$, $B = 0.4$, $D = 0.5$ and results are given for flows $10^3 \leq Ra \leq 10^7$. When $Ra = 10^3$, heat transfer mechanism is dominated by conduction. Also, there is forced convection caused by the moving lid. So, both natural and forced convection have effects on variables stream function, vorticity and temperature. From the streamlines it can be seen that there are two circular vortex occur in the cavity which are called primary vortex (bigger one at the right side of the cavity) and secondary vortex (small one at the left bottom corner of the cavity). While the primary vortex takes the negative value and the secondary vortex takes the positive value. Also they take the minimum and maximum values at their center. The vorticity action, especially near the upper left and upper right corners, occurs all part of the cavity. As the Rayleigh number increases, the secondary vortex of streamline grows and the primary vortex becomes smaller. When the Rayleigh number achieves to 10^7 the vortices become equal in size with opposite direction. Behind this the intensity of streamlines increases as Rayleigh number increases. Similar behavior is seen in the vorticity by forming two vortices at the left and the right side of the cavity. Temperature contour lines start near the heater and distribute towards the other walls for lower values of Rayleigh number but as Rayleigh number increases they concentrate near the heat source. All these behaviors are expected. Because as Rayleigh number increases, convection starts to dominate the heat transfer mechanism. Also, when Rayleigh number takes the higher values, the effect of forced convection disappears completely which is the reason of symmetric behavior of streamlines and vorticity.

5. Conclusion

In this study, DRBEM solution of mixed convection flow in a square cavity with a moving lid on the top, partially heated from below and filled with Cu -water nanofluid is presented by investigating the effect of physical parameters on the flow behavior. DRBEM is a boundary discretization method and has advantages over the domain discretization methods. DRBEM does not show any special form like domain discretization methods and they are full matrices. But because of boundary only discretization, their sizes are smaller by comparing the domain discretization methods.

Beside this, in order to obtain the results for large Rayleigh and Reynolds numbers, it is need to use the smaller time step Δt . When the fundamental solution of the modified Helmholtz equation is used instead of the fundamental solution of Laplace equation for the solution of vorticity transport and temperature equations, it is possible to use the smaller Δt due to the behavior of $K_0(x) \rightarrow 0$ for large x , since $\lambda_w^2 = Re \frac{\rho_n f (1 - \phi)^{2.5}}{\rho_f \Delta t \theta_w}$ and $\lambda_T^2 = Pr Re \frac{\alpha_f}{\alpha_n f \Delta t \theta_T}$. Hence, it is enough to use smaller number of boundary elements by taking smaller Δt . Therefore, in the computations, DRBEM with the fundamental solution of modified Helmholtz equation needs considerably less boundary elements and thus computational cost is noticeably less by comparing the DRBEM with the fundamental solution of Laplace equation.

Also, the idea of using the modified Helmholtz equation as the governing equations for the vorticity transport and temperature equations eliminates the need of another time integration scheme and by using this way the stability problems are eliminated. It is enough to choose proper Δt to obtain stable solution. Because, at the beginning of the process the time derivatives are approximated using forward time discretization method. When any time integration scheme (forward difference or any other) is used inside of the DRBEM procedure, we cannot use fundamental solution of modified Helmholtz equation and so we lose its advantages. This transformations are done at the beginning of the solution procedure to obtain modified Helmholtz equation. On the other hand, there is no difference in the DRBEM idea while the discretization of time derivative is done at the beginning or in the middle of the solution procedure. But, when the time derivative is approximated inside of the solution procedure, we obtain a linear system. In order to satisfy the stability of the obtained system the real part of each of the eigenvalues of the coefficient matrices should be negative. So it requires extra conditions for stability and this is more complicated than the method mentioned here.

Numerical results are given using graphs and tables comparing with the previously published papers and they are in good agreement with the results given in [15].

References

- [1] E. Abu-Nada and A.J. Chamkha, *Mixed convection flow in a lid-driven inclined square enclosure filled with a nanofluid*, Eur. J. Mech. B Fluids, **29**, 472–482, 2010.
- [2] A. Alsoy-Akgün and M. Tezer-Sezgin, *DRBEM solution of the thermo-solutal buoyancy induced mixed convection flow problems*, Eng. Anal. Bound. Elem. **37**, 513–526, 2013.
- [3] A. Alsoy-Akgün and M. Tezer-Sezgin, *DRBEM and DQM solution of natural convection flow in cavity under a magnetic field*, Prog. Comput. Fluid Dyn. **13**, 270–284, 2013.
- [4] A.A.A. Arani, J. Amani and M.H. Esfaha, *Numerical simulation of mixed convection flows in a square double lid-driven cavity partially heated using nanofluid*, J. Nanostruct. **2**, 301–311, 2012.
- [5] M. Bouchmel, B. Nabil, A.M. Ammar, G. Kamel and O. Ahmed, *Entropy generation and heat transfer of Cu-water nanofluid mixed convection in a cavity*, Int. J. Mech. Aerosp. Ind. Mech. and Manuf. Eng. **8**, 2137–2143, 2014.
- [6] C.A. Brebbia, *The boundary element method for engineers*, Pentech Press, 1984.
- [7] A.J. Chamkha and E. Abu-Nada, *Mixed convection flow in single- and double-lid driven square cavities filled with water- Al_2O_3 nanofluid: Effect of viscosity models*, Eur. J. Mech. B Fluids, **36**, 82–96, 2012.

- [8] M.H. Esfe, M. Akbari and A. Karimipour, *Mixed convection in a lid-driven cavity with an inside hot obstacle filled by an Al_2O_3 -water nanofluid*, J. Appl. Mech. Tech. Phys. **56**, 443–453, 2015.
- [9] B. Ghasemi and S.M. Aminossadati, *Mixed convection in a lid-driven triangular enclosure filled with nanofluids*, Int. Commun. Heat Mass, **37**, 1142–1148, 2010.
- [10] S. Gümğüm and M. Tezer-Sezgin, *DRBEM solution of mixed convection flow of nanofluids in enclosures with moving walls*, J. Comput. Appl. Math. **259**, 730–740, 2014.
- [11] S. Hussain, S. Ahmad, K. Mehmood and M. Sagheer, *Effects of inclination angle on mixed convective nanofluid flow in a double lid-driven cavity with discrete heat sources*, Int. J. Heat Mass Tran. **106**, 847–860, 2017.
- [12] S. Kakaç and A. Pramuanjaroenkij, *Review of convective heat transfer enhancement with nanofluids*, Int. J. Heat Mass Tran. **52**, 3187–3196, 2009.
- [13] M. Kalteh, K. Javaherdeh and T. Azarbarzin, *Numerical solution of nanofluid mixed convection heat transfer in a lid-driven square cavity with a triangular heat source*, Powder Technol. **253**, 780–788, 2014.
- [14] M. Mahmoodi, *Mixed convection inside nanofluid filled rectangular enclosures with moving bottom wall*, Therm. Sci. **15**, 889–903, 2011.
- [15] M.A. Mansour, R.A. Mohamed, M.M. Abd-Elaziz and S.E. Ahmed, *Numerical simulation of mixed convection flows in a square lid-driven cavity partially heated from below using nanofluid*, Int. Commun. Heat Mass, **37**, 1504–1512, 2010.
- [16] M. Muthamilselvan, P. Kandaswamy and J. Lee, *Heat transfer enhancement of copper-water nanofluids in a lid-driven enclosure*, Commun. Nonlinear Sci. Numer. Simulat. **15**, 1501–1510, 2010.
- [17] R.K. Nayak, S. Bhattacharyya and I. Pop, *Numerical study on mixed convection and entropy generation of Cu-water nanofluid in a differentially heated skewed enclosure*, Int. J. Heat Mass Tran. **85**, 620–634, 2015.
- [18] H. Nematı, M. Farhadi, K. Sedighi, E. Fattahi and A.A.R. Darzi, *Lattice Boltzmann simulation of nanofluid in lid-driven cavity*, Int. Commun. Heat Mass, **37**, 1528–1534, 2010.
- [19] P.W. Partridge, C.A. Brebbia and L.C. Wrobel, *The dual reciprocity boundary element method*, Computational Mechanics Publications, 1992.
- [20] M.M. Rahman, M.M. Billah, M. Hasanuzzaman, R. Saidur and N.A. Rahim, *Heat transfer enhancement of nanofluids in a lid-driven square enclosure*, Numer. Heat Tr. A-Appl. **62**, 973–991, 2012.
- [21] M.M. Rahman, M.M. Billah, A.T.M.M. Rahman, M.A. Kalam and A. Ahsan, *Numerical investigation of heat transfer enhancement of nanofluids in an inclined lid-driven triangular enclosure*, Int. Commun. Heat Mass, **38**, 1360–1367, 2011.
- [22] R. Saidur, K.Y. Leong and H.A. Mohammad, *A review on applications and challenges of nanofluids*, Renew. Sust. Energ. Rev. **25**, 1646–1668, 2011.
- [23] M. Salari, M.M. Tabar, A.M. Tabar and H.A. Danes, *Mixed convection of nanofluid flows in a square lid-driven cavity heated partially from both the bottom and side walls*, Numer. Heat Tr. A-Appl. **62**, 158–177, 2012.
- [24] M.A. Sheremet and I. Pop, *Mixed convection in a lid-driven square cavity filled by a nanofluid: Buongiorno's mathematical model*, Appl. Math. Comput. **266**, 792–808, 2015.
- [25] F. Talebi, A.H. Mahmoudi and M. Shahi, *Numerical study of mixed convection flows in a square lid-driven cavity utilizing nanofluid*, Int. Commun. Heat Mass, **37**, 79–90, 2010.
- [26] R.K. Tiwari and M.K. Das, *Heat transfer augmentation in a two-sided lid-driven differentially heated square cavity utilizing nanofluids*, Int. J. Heat Mass Tran. **50**, 2002–2018, 2007.

- [27] X.Q. Wang and A.S. Mujumdar, *A review on nanofluids-part I:Theoretical and numerical investigations*, Braz. J. Chem. Eng. **25**, 613–630, 2008.
- [28] X.Q. Wang and A.S. Mujumdar, *A review on nanofluids-part II:Experiments and applications*, Braz. J. Chem. Eng. **25**, 631–648, 2008.
- [29] D. Wen, G. Lin, S. Vafaei and K. Zhang, *Review of nanofluids for heat transfer applications*, Particuology, **7**, 141–150, 2009.
- [30] W. Yu, D.M. France, J.L. Routbort and S.U.S. Choi, *Review and comparison of nanofluid thermal conductivity and heat transfer enhancements*, Heat Transfer Eng. **29**, 432–460, 2008.